Chapter 2
Suprathermal Populations and Their Effects in Space Plasmas: Kappa vs. Maxwellian

Viviane Pierrard, Marian Lazar, and Milan Maksimovic

Abstract Understanding the origin and implications of the suprathermal particle populations present in space plasmas is facilitated by the observations and theoretical interpretations using Kappa distribution models. Characteristic to collision-poor plasmas, such as the solar wind and planetary environments, suprathermal populations may significantly contribute to the energy budget of electrons and ions, with consequences on their temperature, bulk velocities, and the heat flux. Moreover, if present at low altitudes in the solar atmosphere, suprathermal particles can trigger the process of velocity filtration to explain coronal overheating, while the exospheric solar wind models of Kappa distributed populations are also able to predict the acceleration of fast streams (even originating in coronal holes). The present chapter reviews these concepts and physical properties on the basis of recent interpretations using comparisons between models based on Maxwellian and on Kappa distributions which bring improved and realistic perceptions of suprathermal plasma particles.

V. Pierrard (✉)
Royal Belgian Institute for Space Aeronomy (BIRA-IASB), Space Physics, Solar Terrestrial Center of Excellence (STCE), Brussels, Belgium

Center for Space Radiations (CSR) and Georges Lemaitre Centre for Earth and Climate Research (TECLIM), Earth and Life Institute (ELI), Université Catholique de Louvain (UCLouvain), Louvain-La-Neuve, Belgium
e-mail: viviane.pierrard@aeronomie.be

M. Lazar
Centre for Mathematical Plasma Astrophysics, KU Leuven, Leuven, Belgium

Institut für Theoretische Physik, Lehrstuhl IV: Weltraum- und Astrophysik, Ruhr-Universität Bochum, Bochum, Germany
e-mail: marian.lazar@kuleuven.be

M. Maksimovic
LESIA, Observatory of Paris Meudon, Paris, France

M. Lazar, H. Fichtner (eds.), *Kappa Distributions*, Astrophysics and Space Science Library 464, https://doi.org/10.1007/978-3-030-82623-9_2

2.1 Introduction: Empirical Kappa Models

The Kappa distribution function has been introduced as an empirical model to describe accurately the velocity distributions and energy fluxes of plasma particles observed in terrestrial magnetosphere and solar wind (Olbert 1968; Vasyliunas 1968; Christon et al. 1989; Collier et al. 1996; Maksimovic et al. 1997b; Nicolaou et al. 2020). Reviews of earlier applications of Kappa distributions in observations and theoretical modeling can be found in Pierrard and Lazar (2010) and Lazar et al. (2012b).

A Kappa distribution has a nearly Maxwellian core at low energies, and high-energy tails decreasing as suprathermal power laws that can be significantly broader than exponential tails; Fig. 2.1 below shows that a Kappa distribution function can reproduce the electron distributions up to 1 keV much better than a combination of two Maxwellians (Maksimovic et al. 1997b). This contrast is also highlighted by the break-point energy (or velocity) between the core and suprathermal tails (Maksimovic et al. 2005; Bakrania et al. 2020), strongly suggesting the existence of at least two distinct populations, i.e., a quasi-thermal core and a suprathermal component that enhances the high-energy tails and incorporates the so-called halo (Maksimovic et al. 2005) but also the more asymmetric beaming or strahl populations (Berčič et al. 2019). Statistics of solar wind electrons have shown that both halo and strahl break-point energies display a significant increase with core temperature, and both decrease with increasing solar wind speed (the halo break-point energy shows distinct profiles above and below 500 km s^{-1}, apparently related to different fast and slow wind origins) (Bakrania et al. 2020).

Such observational evidence suggests that Kappa distribution functions can also be employed for partial fits, to describe only the suprathermal tails in the observed distributions (Maksimovic et al. 2005; Štverák et al. 2008; Wilson-III et al. 2019). In such a case, the overall fitting models combine a Maxwellian core with a Kappa halo, and, eventually, a drifting-Kappa to reproduce the beaming or strahl populations, see also Figs. 2.1 and 2.2 below. By contrast to a single (or global) Kappa distribution, multi-component models provide more accurate fits to the observations, especially for the highly asymmetric distributions in the presence of strahls, which are aligned to the magnetic field in the anti-sunward direction. Due to its asymmetry, the strahl can be separated from the core and halo populations, which remain to be described by dual models summing up a bi-Maxwellian core and bi-Kappa halo, and quantifying the main properties of these populations, like number densities and anisotropic temperature components, parallel and perpendicular to the local magnetic field (Maksimovic et al. 2005; Štverák et al. 2008; Lazar et al. 2017). In Sect. 2.2.2 we refer to recent observational interpretations which invoke these properties of solar wind electrons in the ecliptic (Pierrard et al. 2016; Lazar et al. 2020b; Pierrard et al. 2020).

Kappa models have also been invoked in studies of ion velocity distributions or their energy fluxes in space plasmas, in general, for partial descriptions of energetic populations (including pickup ions and v^{-5} suprathermals), with energies much

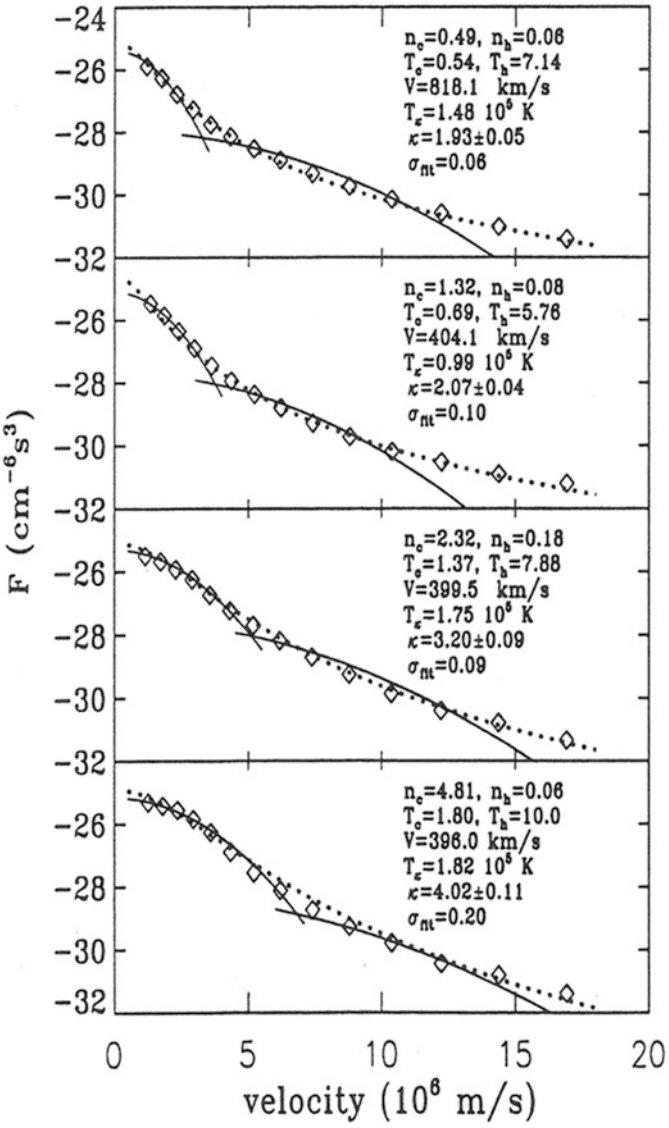

Fig. 2.1 Ulysses observations of electron velocity distributions (averaged over all pitch-angles) shown with diamonds are better fitted by a Kappa distribution function (dotted line) than a sum of two Maxwellians (solid lines). The core is well fitted by a cooler Maxwellian (subscript 'c'), but suprathermal tails are not reproduced by the second, hotter Maxwellian (subscript 'h'). The corresponding parameters from fitting, i.e., number densities n in cm^{-3}, temperatures in units of 10^5 K, power exponent κ, as well as their (maximum) deviations σ_m are given in the legends. Reproduced with permission from Maksimovic et al. (1997b). © John Wiley and Sons

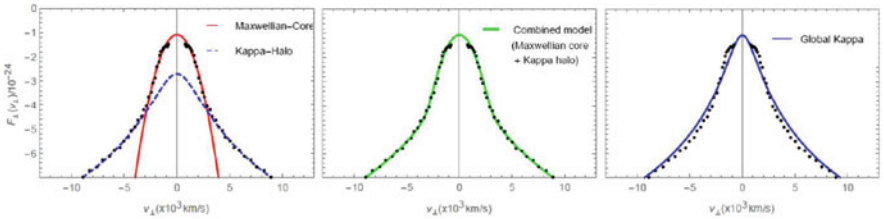

Fig. 2.2 Left panel: electron velocity distribution shown with dots (symmetric perpendicular cut) is fitted by a Maxwellian core (solid red) and a Kappa halo (dashed blue). The resulting dual fit (green) in the middle panel is more accurate than a global Kappa fit (solid blue) in the right panel. Credit: Lazar et al. (2017), reproduced with permission ©ESO

higher than 1 keV (Christon et al. 1989; Chotoo et al. 2000; Eyelade et al. 2021; Fisk and Gloeckler 2014). These are spectra of protons and heavier ions in the solar wind (Chotoo et al. 2000), and planetary environments (Eyelade et al. 2021). From earlier studies, only a few have described the halo population of ions with energies below 1 keV (Collier et al. 1996). There are, however, recent works attempting to provide statistics of proton and ion properties on the basis of an extended Kappa representation of their energy spectra measured in planetary magnetospheres (Sun et al. 2018). Preliminary results show that 3/4 of the proton spectra measured on Mercury's orbit are well described by Kappa distributions, promising capabilities to estimate their density, temperature and κ parameter (James et al. 2020).

Multi-component fitting models have also been refined in recent years, by exploiting various anisotropic Kappa functions able to accurately characterize the suprathermal halo and beaming populations (Berčič et al. 2019). It became thus possible to estimate the low relative drifts that electron core and halo populations may exhibit in the solar wind frame (Wilson-III et al. 2019). Moreover, previous indirect methods used to quantify the electron strahl can now be tested and complemented by direct fitting with complex bi-Kappa distributions with a drift parallel to the magnetic field (drifting bi-Kappa) to certify their main properties, like density, relative drift (velocity) and temperature, but reveal also intrinsic details of their temperature anisotropy (Wilson-III et al. 2019; Wilson et al. 2019). Such a detailed parametrization is vital for modeling and understanding plasma processes like, for instance, the energy and heat transport, or the wave instabilities self-generated by the kinetic anisotropies of plasma particles. Suprathermal populations drifting or beaming ahead the bulk solar wind are responsible for the main heat flux transported in the heliosphere. Recent estimates of the electron pressure and heat flux have shown that only a simplified Maxwellian modeling of Kappa distributed populations may lead to significant underestimations (Lazar et al. 2020a). Moreover, by introducing the new regularized Kappa distribution (see also the discussions in the chapter by Scherer et al.), such macroscopic properties can now be evaluated for a stronger presence of suprathermals associated to low values of $\kappa < 3/2$, that would not have been possible with a standard Kappa representation (Lazar et al. 2020a; Scherer et al. 2017). On the other hand, kinetic instabilities and the

enhanced wave fluctuations are expected to play multiple key roles in collision-poor plasmas (Shaaban et al. 2018; López et al. 2020); details about their properties in the presence of Kappa-distributed populations can be found in chapters by Shaaban et al., and Lopez et al. in Part IV of this book.

2.2 Kappa-Distributed Electrons in the Solar Wind

In this section we discuss the electron suprathermal populations observed in the solar wind and planetary plasmas, whose level of knowledge and understanding from Kappa modeling is at the most advanced stage.

2.2.1 Insights from Kappa Modeling

Motivated by the high contrast between the low-energy core and suprathermal tails of the observed distributions, dual or multi-component models involve Kappa distribution functions to reproduce only the suprathermal populations, like halo and strahl electrons (Maksimovic et al. 2005; Štverák et al. 2008; Berčič et al. 2019; Wilson-III et al. 2019). Some of these studies of solar wind electrons have fitted the halo component with a bi-Kappa distribution function (Maksimovic et al. 2005; Štverák et al. 2008; Berčič et al. 2019)

$$f_\kappa(v_\parallel, v_\perp) = \left[\frac{m}{\pi k_B(2\kappa-3)}\right]^{3/2} \frac{1}{T_\perp\sqrt{T_\parallel}} \frac{\Gamma(\kappa+1)}{\Gamma(\kappa-1/2)} \times \left[1+\frac{m}{k_B(2\kappa-3)}\left(\frac{v_\parallel^2}{T_\parallel}+\frac{v_\perp^2}{T_\perp}\right)\right]^{-\kappa-1}, \tag{2.1}$$

which is expressed, in contrast to the Olbertian (bi-)Kappa version, see the introduction chapter, in terms of the κ parameter and the components of (kinetic) temperature $T_{\parallel,\perp}$, directly defined by the second order moments of this distribution function

$$T_\parallel \equiv \frac{m}{k_B}\int d^3v v_\parallel^2 f_\kappa(v_\parallel, v_\perp), \quad T_\perp \equiv \frac{m}{2k_B}\int d^3v v_\perp^2 f_\kappa(v_\parallel, v_\perp). \tag{2.2}$$

This version of a Kappa distribution suggests that κ and $T_{\parallel,\perp}$ can be independent, as speculated in some studies attempting to justify this notion of non-equilibrium temperature also thermodynamically, by associating it with Maxwellian limit

$$f_{\kappa\to\infty}(v_\parallel, v_\perp) = \left(\frac{m}{2\pi k_B}\right)^{3/2} \frac{1}{T_\perp\sqrt{T_\parallel}} \exp\left[-\frac{m}{2k_B}\left(\frac{v_\parallel^2}{T_\parallel}+\frac{v_\perp^2}{T_\perp}\right)\right]. \tag{2.3}$$

Kappa-distributed plasmas are, however, out of thermal equilibrium and a macroscopic modeling needs a rigorous elaboration on the basis of the principal velocity moments (for related discussions, see also other chapters of this book). Instead, to fit the observations, the same Kappa version from Eq. (2.1) does not necessarily need to assume κ and $T_{\parallel,\perp}$ independent, but it takes the advantage of providing directly the fitting values for the (anisotropic) components of temperature.

Later studies of these kinetic temperatures have proved their direct dependency of the power exponent κ (Lazar et al. 2017), as the one indicated by the Olbertian version of Kappa (Olbert 1968; Vasyliunas 1968)

$$T_{\parallel,\perp} = \frac{\kappa}{\kappa - 3/2} \frac{m\theta^2_{\parallel,\perp}}{2k_B}, \tag{2.4}$$

where $\kappa > 3/2$ and $\theta \simeq \sqrt{2k_B T_M/m}$ is the most probable speed or thermal speed characteristic to the Maxwellian limit of the Olbertian version. Scatter plots from Fig. 2.3 represent the components of halo temperature (subscript 'h') as a function of κ, from electron measurements in Štverák et al. (2008). Overplotted with dashed lines are temperature components depending on κ via the Eqs. (2.4), and decreasing asymptotically to an average value $T^{(a)}_{M,\parallel,\perp} = 5 \times 10^5$ K, where $k_B T^{(a)}_{M,\parallel,\perp}$ corresponds identically to $m\theta^2_{\parallel,\perp}/2$. The variations of temperature components are given by the limits between which these data fall. Lowest variations, i.e., more concentrated data points, are specific to high values of κ signifying a more thermalized halo, encountered at low heliospheric distances (Maksimovic et al. 2005; Pierrard et al. 2016). The halo temperature increases and the spread of its values becomes wider for lower values of κ (Lazar et al. 2017), which are obtained with increasing distance from the Sun, especially beyond 1 AU (Maksimovic et al. 2005; Pierrard et al. 2016). Total temperatures $T_h = T_{h,\parallel}/3 + 2T_{h,\perp}/3$ and $T_M = T_{M,\parallel}/3 + 2T_{M,\perp}/3$ are conditioned by the same relationship (2.4).

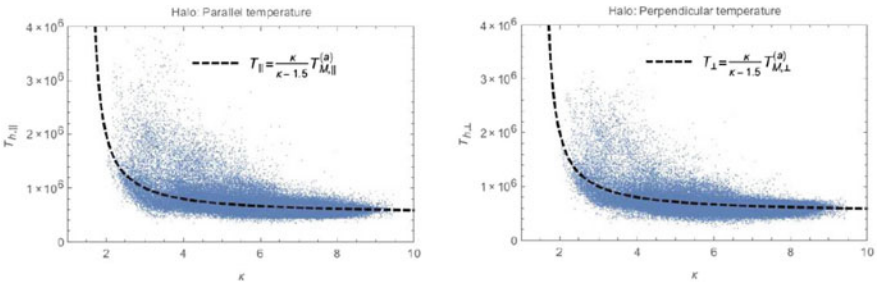

Fig. 2.3 Scatter plots (blue dots) of the components of halo temperature $T_{h,\parallel}$ (top) and $T_{h,\perp}$ (bottom) as a function of κ, from the observations of electron solar wind distributions. Overplotted with dashed lines are temperature components given by Eq. (2.4). Credit: Lazar et al. (2017), reproduced with permission ©ESO

These results outline the importance of the Kappa distribution function in the form originally introduced by Olbert (1968). This form ensures a correct physical representation of the Kappa distributed populations, enabling a consistent definition of temperature (by the second order moment), as a physical quantity dependent on the power exponent κ via a relationship $T = T(\kappa)$ given by (2.4). This mean kinetic energy, or kinetic temperature, is naturally enhanced by the presence of suprathermals in the high energy tails of Kappa distribution (quantified by a finite κ). The Maxwellian limit (subscript M) of lower temperature used for comparison, i.e., $T(\kappa) > T(\kappa \to \infty) = T_M$, should correspond to the plasma state reached after relaxation, i.e., in the absence of source of energy entertaining the suprathermals (see also the discussions in the chapter by Effenberer and Jeffreys).

For a global Kappa representation, which incorporates not only suprathermal tails but also the low-energy core (Vasyliunas 1968), these contrasting features become even more evident, but also practical. In such a case, the Maxwellian limit of lower temperature approaches the quasi-thermal core of Kappa distributed population (Lazar et al. 2015, 2016), and facilitates the contrast with suprathermal tails. Comparison between Kappa and its Maxwellian core becomes straightforward, and can be invoked to outline the presence of suprathermals and understand how these population influences various properties and physical processes of space plasmas (see the effects of suprathermals on the kinetic instabilities, described in the chapter by Shaaban et al.).

2.2.2 *Properties of Halo Electrons*

Adequate representation using Kappa models allows a detailed characterization of the halo component of solar wind electrons, as well as the implications of this population in the solar corona and the heliosphere (Maksimovic et al. 2005; Štverák et al. 2008; Pierrard et al. 2016; Lazar et al. 2020b; Pierrard et al. 2020). Figure 2.4

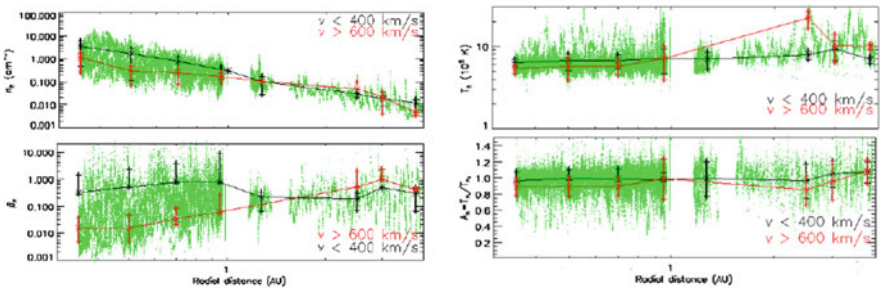

Fig. 2.4 Electron halo properties measured in the ecliptic with average values and their standard deviations estimated for the slow (black) and fast (red) winds. Credit: Lazar et al. (2020b), reproduced with permission ©ESO

displays the variations with heliospheric distance (from 0.3 to 4 AU) for the main properties of electron halo population, i.e., number density, temperature, plasma beta, and temperature anisotropy. The average data and their standard deviations are overplotted with black for the slow winds with $V < 400$ km/s, and with red for the fast winds with $V > 600$ km/s.

Thus, at relatively low radial distances, i.e., <1 AU, all the parameters characterizing the halo electrons show a clear anticorrelation with the solar wind speed, in agreement with the hypothesis that low- and high-speed streams have different sources. It is indeed measured that plasmas from coronal holes, where high-speed streams are believed to originate, have densities and temperatures below those estimated in a more homogeneous corona (Maksimovic et al. 2020). Near the Sun, at distances $\gtrsim$0.3 AU, the halo electrons show a higher suprathermalization, i.e., lower values of κ in the fast winds (Lazar et al. 2020b). Corroborated with the origin of fast winds, these observations support the hypothesis that suprathermal electrons, and eventually ions, are present in the lower corona, and can, thus, contribute to a coronal overheating by velocity filtration (Scudder 1992a; Meyer-Vernet 2007), and, implicitly, to the solar wind acceleration (Zouganelis et al. 2005). Detailed discussions of the processes involved can be found below in the present chapter.

With increasing distance from the Sun, this contrast triggered by a bi-modal solar wind decreases, and may even switch to a positive correlation beyond 1 AU (Lazar et al. 2020b). In general, the parameter κ decreases with heliocentric distance, suggesting the existence of a suprathermalization or energization of electrons by interaction with kinetic plasma waves and turbulent fluctuations, counteracting collisions which become less efficient with increasing distance from the Sun (Pierrard et al. 2011). Somewhat stronger in the fast winds, this suprathermalization can be stimulated by the wave fluctuations self-generated by the strahl (or heat-flux) instabilities associated with energetic streams. Sufficiently hot and tenuous, these suprathermal populations should be collisionless (Wilson-III et al. 2019; Wilson III et al. 2018). Scenarios invoking collisions or collisional age of plasma particles may nicely apply to core electrons to explain their accumulation near quasi-equilibrium states of isotropic temperature (Štverák et al. 2008). A similar accumulation of suprathermal halo electrons near isotropy (Štverák et al. 2008) should result not only from reminiscences of a more thermalized halo (high values of $\kappa > 5$) in the outer corona (Maksimovic et al. 2005; Pierrard et al. 2016), but mainly from constraining the effects of the anisotropy driven instabilities (Štverák et al. 2008).

A steeper decrease of κ in the slow winds beyond 0.7 AU has been explained by the decline of collisions and their thermalization effect with increasing distance from the Sun (Lazar et al. 2020b). This is apparently correlated with a similar decrease of density, black line in Fig. 2.4, top panel, especially beyond 1 AU, suggesting that solar wind expansion may also induce an effective suprathermalization of the halo electrons. In the slow winds, the halo temperature (black line in Fig. 2.4, top-second panel) exhibits a modest increase consistent with the variation of κ (see also Lazar et al. 2017).

On the other hand, the main properties of electron halo show highly non-monotonic variations in the fast winds (see Fig. 2.4). This population appears to

be more affected by transient events, under the influence of more pronounced strahls, e.g., self-generated instabilities, or even more energetic events, such as coronal mass ejections (CMEs). At low distances, the halo does not gain much from a redistribution of strahl electrons, and the number density (n_h) decreases steeply with the solar wind expansion. This trend is tempered with increasing radial distance, for instance beyond 0.5 AU, when the adiabatic focusing weakens and cannot counteract the pitch-angle scattering of strahl electrons by the self-induced wave fluctuations.

In fast winds, the halo temperature (T_h, Fig. 2.4, top-second panel) and the plasma beta (β_h, Fig. 2.4, third panel) show similar radial profiles. These two parameters increase with heliocentric distance, especially beyond 0.5 AU, which suggests a subsequent energization induced by the interaction with the self-enhanced wave fluctuations. This tendency is drastically accentuated after 1.3 AU, apparently, by a transient energetic event, like a CME, peaking the values of these parameters at 2.7 AU for T_h and 3.0 AU for β_h (Lazar et al. 2020b). The increase of these parameters saturates at and beyond 3.0 AU. The presence of a CME is supported by a series of specific signatures in observational data, as shown by a relative increase of number density and temperature, or the presence of counterbeaming strahls in the closed magnetic field loops of a CME, in our case mimicking an effective temperature anisotropy $T_{h,\parallel} > T_{h,\perp}$. These scenarios are also supported by complementary studies of solar wind electrons. For instance, similar fast wind data collected by Ulysses but from high latitudes show a substantial scattering of the electron strahl in the same radial interval 1.3–3.0 AU (Hammond et al. 1996). Another study combining fast wind data from ecliptic and high-latitudes has shown that the relative density of halo electrons already starts to increase at 0.5 AU, and on the expense of the strahl relative density (Maksimovic et al. 2005). All together these results show a progressive enhancement of halo electrons and their properties in the fast winds, especially between 0.5 AU and 3.0 AU, supporting the idea that already at that distance significant fractions of strahl electrons and their energy begin to be redistributed to the halo population.

2.2.3 Properties of Strahl Electrons

Earlier studies have shown an electron strahl or beaming population (subscript 'b') more prominent in the high-speed winds, with narrower angular widths and higher densities (Maksimovic et al. 2005; Anderson et al. 2012). The asymmetric strahl can be isolated by subtracting the dual core-halo fit from the measured distribution, and many of its properties are found to be energy dependent. Thus, the pitch-angle width (PAW) of low-beta strahls ($\beta < 0.2$, e.g., in the outer corona) conforms to a collisionless focusing model, while in the high-beta ($\beta > 0.4$) winds the strahl broadens with increasing the distance from the Sun, as if scattered by the self-generated wave instabilities (Berčič et al. 2019), since suprathermal electrons are collision-poor (Wilson et al. 2019); see also the discussions in chapter by

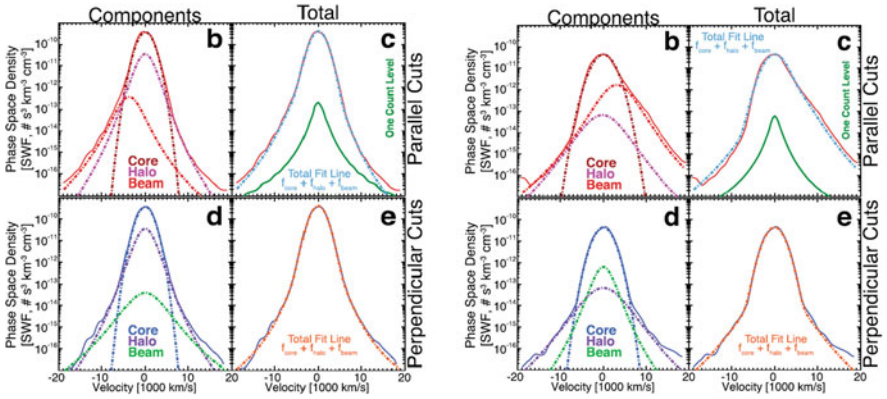

Fig. 2.5 Electron distributions from two events captured by Wind with halo and strahl components described by anisotropic Kappa models. Top panels show a regular strahl weaker than halo, and Bottom panels display an event with a stronger strahl. Reproduced with permission from Wilson-III et al. (2019). © AAS

Vocks. More valuable details have been obtained from fitting the electron beams with drifting bi-Kappa distribution functions (Wilson-III et al. 2019; Wilson et al. 2019), see also Fig. 2.5, strengthening and improving the existing knowledge of their properties, e.g., densities, relative drifts, temperature and temperature anisotropy. Fitting models used in these extended observational analyses have included drifts in both parallel and perpendicular directions, and the results have shown that electron strahls are, in general, well aligned to the magnetic field direction. High density strahls stronger than halo (subscript 'h') population, satisfying $n_b > n_h$, are typical to fast solar winds, see bottom panels in Fig. 2.5. From the same statistics of solar wind electrons at 1 AU (often affected by shocks), the electron beam/strahl may also exhibit an intrinsic temperature anisotropy $A_b = T_{b,\perp}/T_{b,\parallel}$ with a variation $0.13 \leqslant A_b \leqslant 15.2$ slightly larger than suprathermal halo. But, as for the suprathermal halo, the highest number of events concentrates near the isotropy condition ($A_b = 1$), with a weak tendency towards $A_b < 1$, and a moderately low plasma beta parameter $\beta_{b,\parallel} \simeq 0.1$, specific to suprathermal populations (see also the electron halo) usually with low number densities.

In closed magnetic field topologies, the electron distributions may show double-strahls or counter-beaming populations, more or less symmetric, see Lazar et al. (2012a) and references therein. Guided by the magnetic field lines, these double strahls are captured when the spacecraft passes through magnetic loops of the CMEs, co-rotating interaction regions (CIRs) of fast and slow winds, or interplanetary shocks. Unfortunately, counter-beaming strahls make it difficult to distinguish them from the other core and halo populations and fit them to any model distribution (Lazar et al. 2014). Moreover, in the presence of (symmetric) double strahls, the overall shape of the observed distribution mimics an anisotropic temperature T with $T_\parallel > T_\perp$, but with suprathermal tails more skewed than a bi-Kappa distribution,

better reproduced by a product-bi-Kappa fit (Lazar et al. 2012a); more details and a comparison of these anisotropic Kappa models can be found in (Summers and Thorne 1991).

2.3 Consequences of Kappa-Distributed Suprathermals

In the following, we compare the results obtained with different velocity distribution functions (VDFs) for particles in neutral or ionized atmospheres or in space plasmas. These VDFs are (i) a Maxwellian, (ii) a sum of two Maxwellians, (iii) a single Kappa distribution and (iv) a sum of a Maxwellian and a Kappa. This method allows us to show the main characteristics of these distributions and of the profiles of their moments (number density, flux, temperature and heat flux) in planetary and stellar atmospheres, illustrated here by specific applications to the solar atmosphere.

2.3.1 Atmospheres in Hydrostatic Equilibrium. Isotropic Kappa

In an atmosphere in hydrostatic equilibrium, the flux of escaping particles is null, as well as their global bulk velocity. In neutral atmospheres, the observations show generally Maxwellian distributions for the particles:

$$f_M(r_0, v) = n_0 \left(\frac{m}{2\pi k_B T_0}\right)^{3/2} \exp\left(-\frac{mv^2}{2k_B T_0}\right) = N_0 \exp\left(-\frac{mv^2}{2k_B T_0}\right) \tag{2.5}$$

with m the mass of the particles, T_0 their temperatures, v their velocity, k_B the Boltzmann constant, and n_0 the density at the radial distance r_0.

In space plasmas, like the solar wind for instance, the VDFs of the charged particles are generally not observed to be Maxwellian (Pierrard and Lazar 2010 for a review). The VDFs of the different particle species have more suprathermal particles in their tails. As already mentioned, Kappa distributions well fit such distributions in space plasmas:

$$f_\kappa(r_0, v) = n_0 \left(\frac{m}{2\pi k_B T_0}\right)^{3/2} \frac{\Gamma(\kappa+1)}{\kappa^{3/2}\Gamma(\kappa-1/2)} \left(1 + \frac{mv^2}{2k_B T_0 \kappa}\right)^{-\kappa-1} \tag{2.6}$$

with tails decreasing as a power law with the square velocity, and the κ parameter controlling the power law tails. When κ tends to infinity, the Kappa VDF becomes identically Maxwellian, while low κ corresponds on the contrary to high suprathermal tails. Figure 2.1 shows examples of Kappa distributions (dotted lines) with high suprathermal tails in comparison to Maxwellian cores (solid lines at low velocities)

with the same T_0 core population to fit observed solar wind Ulysses observations (diamonds).

There are different origins that can explain the Kappa tails (see Pierrard and Lazar 2010 and other chapter of the present book) but it seems related to Coulomb interactions that are more efficient for low energy particles than for high energy ones. Generalizations of thermodynamics based on the Tsallis non-extensive entropy formalism (Tsallis 1995) indicate that Kappa distributions can result from a new generalized Lorentzian statistical mechanics formulated for a collisionless plasma far from thermal (Boltzmann-Maxwell) equilibrium, but containing turbulence in quasi-stationary equilibrium (e.g. Yoon 2020 and references therein). Kappa distributions can also be solution of the Fokker-Planck equation under certain specific conditions, as shown by Shizgal (2018).

Such distributions may be already present at low altitude in ionized planetary and stellar atmosphere (Pierrard and Lemaire 1996), in the region where the collisions are sufficient to maintain an isotropic velocity distribution function, but will not necessarily lead to an exponential decrease of the distribution at high energy. For the solar atmosphere, low altitude corresponds to the region of the chromosphere and low corona, below the exobase (Maksimovic et al. 1997a).

An enhanced energetic population in comparison to the Maxwellian function can also be simulated by a sum of two Maxwellians with different temperatures (a Maxwellian core plus a second, more energetic Maxwellian) (Pierrard 2012b):

$$f_{2\mathrm{M}}(r_0, v) = N_0 \exp\left(-\frac{mv^2}{2k_B T_0}\right) + N_1 \exp\left(-\frac{mv^2}{2k_B T_1}\right) \tag{2.7}$$

using $N_i = n_i(m/(2\pi k_B T_i))^{3/2}$ with $n_0 > n_1$, but $T_0 < T_1$, and thus $N_0 > N_1$. Figure 2.1 shows, in addition to the core Maxwellians, the second Maxwellians with higher temperatures and lower densities that fit the observed suprathermal tails (see solid lines at high velocities).

2.3.2 *The Influence of Altitude on Distributions and Macroscopic Properties*

Velocity Distributions (VDFs)

In the exosphere, the VDFs of the different particle species evolve with the altitude under the effect of the gravity, the electric and magnetic fields. The VDF at a higher altitude r is directly obtained from the VDF at a lower reference altitude r_0 using the Liouville theorem stipulating conservation of energy and conservation of the magnetic moment in case of anisotropic distribution (Pierrard and Lemaire 1996).

For a Maxwelllian distribution

$$f_M(r, v) = n_0 \left(\frac{m}{2\pi k_B T_0}\right)^{3/2} \exp\left(-\frac{mv^2}{2k_B T_0} - q\right) \tag{2.8}$$

with

$$q = \frac{m(\phi(r) - \phi(r_0)) - Ze(V(r) - V(r_0))}{k_B T_0} \tag{2.9}$$

where ϕ is the gravitational potential, V is the electric potential and Ze the charges of the particles.

For a Kappa distribution

$$f_\kappa(r, v) = f_\kappa(r_0, v) = n_0 \left(\frac{m}{2\pi k_B T_0}\right)^{3/2} A_\kappa \left(1 + \frac{mv^2}{2k_B T_0 \kappa} + \frac{q}{\kappa}\right)^{-\kappa-1} \tag{2.10}$$

with

$$A_\kappa = \frac{\Gamma(\kappa + 1)}{\kappa^{3/2}\Gamma(\kappa - 1/2)} \tag{2.11}$$

For a sum of two Maxwellians, using $N_i = n_i(m/(2\pi k_B T_i))^{3/2}$:

$$f_{2M}(r, v) = N_0 \exp\left(-\frac{mv^2}{2k_B T_0} - q_0\right) + N_1 \exp\left(-\frac{mv^2}{2k_B T_1} - q_1\right) \tag{2.12}$$

where q_0 and q_1 refer to Eq (2.9) with the different temperatures T_0 and T_1.

The sum of a Maxwellian for the core and a Kappa function for the halo used to fit the observed VDFs in the solar wind (Štverák et al. 2008) is simply the addition of Eqs. (2.8) and (2.10), and the dependence as a function of the radial distance is given by the sum of the two VDFs. Table 2.1 summarizes the expressions of the different VDFs and their density n and temperature T expressions as a function of the radial distance r (Pierrard and Lemaire 1996; Pierrard 2012b).

Velocity Filtration

Figure 2.6 (left) illustrates the VDF corresponding to a sum of two Maxwellians at a low reference level (black) and at a higher altitude (blue). Since the density is lower, the VDF at higher altitude is below the black line. But, as clearly illustrated in Fig. 2.6, the core (low temperature T_0) Maxwellian decreases faster than the energetic (high temperature T_1) Maxwellian, so that the tails of the distribution are more important at higher altitude. This is called the velocity filtration effect (Scudder 1992a,b). Superposing the two VDFs (by multiplying the blue VDF by a factor so that its maximum is located at 1, like the black one), one can see that the tails are more important than at low altitude (see red VDF), which corresponds also to an increase of the temperature with the altitude because df/dv decreases.

Table 2.1 Names of the VDFs, their expression, density n and temperature T equations as a function of the altitude r

$f(r, v)$	$f(r_0, v)$	$n(r)$	$T(r)$
f_M	$N_0 \exp\left(-\frac{mv^2}{2k_B T_0}\right)$	$n_0 \exp(-q_0(r))$	T_0
f_{2M}	$N_0 \exp\left(-\frac{mv^2}{2k_B T_0}\right) +$	$n_0 \exp(-q_0(r)) +$	$\frac{n_0(r)T_0+n_1(r)T_1}{n_0(r)+n_1(r)}$
	$N_1 \exp\left(-\frac{mv^2}{2k_B T_1}\right)$	$n_1 \exp(-q_1(r))$	
f_κ	$N_0 A_\kappa \left(1+\frac{mv^2}{2k_B T_0 \kappa}\right)^{-\kappa-1}$	$n_0 \left(1+\frac{q_0(r)}{\kappa}\right)^{-\kappa+1/2}$	$T_0 \frac{\kappa}{(\kappa-3/2)} \left(1+\frac{q_0(r)}{\kappa}\right)$
$f_M + f_\kappa$	$N_0 \exp\left(-\frac{mv^2}{2k_B T_0}\right) +$	$n_0 \exp(-q_0(r)) +$	$\frac{n_0(r)T_0+n_1(r)T_1(r)}{n_0(r)+n_1(r)}$
	$N_1 A_\kappa \left(1+\frac{mv^2}{2k_B T_1 \kappa}\right)^{-\kappa-1}$	$n_1 \left(1+\frac{q_1(r)}{\kappa}\right)^{-\kappa+1/2}$	

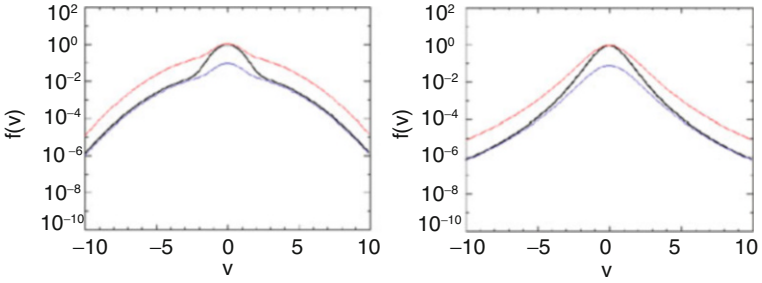

Fig. 2.6 Velocity filtration for a sum of two Maxwellians (left) and a Kappa (right). Here, v is the velocity normalized to the thermal speed $w = \sqrt{2k_B T/m}$. Black: VDF at low radial distance r_0 (e.g., $r_0 = 1.1R_s$), blue: VDF at an upper radial distance r_1 ($= 3R_s$), and red: VDF at r_1 normalized so that the top of the distribution corresponds to the initial distribution, enabling to illustrate the velocity filtration and the temperature increase

When only a single isotropic Maxwellian describes the gas or plasma, then the density decreases exponentially with the radial distance, but the temperature is constant and remains identical for all altitudes (see Table 2.1).

For a sum of two Maxwellians with different temperatures ($T_1 > T_0$), the density of the low temperature Maxwellian decreases faster than the one with high temperature as illustrated in Fig. 2.6. Thus, the temperature increases (see Fig. 2.7), up to a maximum corresponding to T_1. At higher distances, the temperature remains constant.

For an isotropic Kappa distribution, the density decreases as a power law with the radial distance, thus faster than for the Maxwellian with the same T_0. The temperature increases (see Table 2.1) and tends also to a maximum (see Fig. 2.6, 2.7, and 2.8).

Temperature Increase: Coronal Heating

If we considered a neutral atmosphere, only gravity should be taken into account in Eq (2.9) determining $q(r)$. In ionized atmospheres, like for the solar corona, the electric potential has also to be considered in $q(r)$, even if the gravitational potential

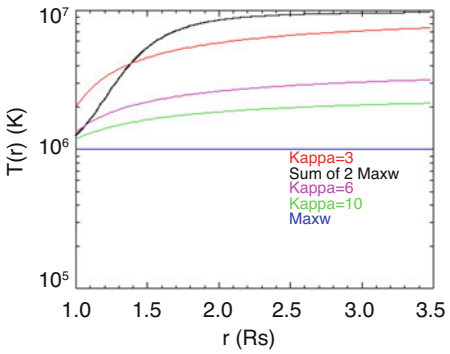

Fig. 2.7 Temperature as a function of radial distance, obtained for different isotropic VDFs assuming $T_0 = 10^6$ K: Maxwellian (blue), sum of two Maxwellians (black), Kappa with $\kappa = 10$ (green), 6 (magenta) and 3 (red)

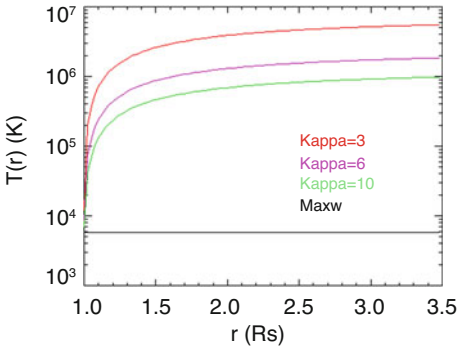

Fig. 2.8 Temperature increase obtained for protons and electrons assuming $T_0 = 6000$ K at $r_0 = 1\mathrm{R_s}$ for different isotropic VDFs: Maxwellian (black), Kappa VDFs with $\kappa = 10$ (green), $\kappa = 6$ (magenta) and $\kappa = 3$ (red)

dominates the electric one at very low altitudes. Let us assume a simple case of an ionized atmosphere in hydrostatic equilibrium composed by electrons and protons that have a same VDF with the same density and temperature $T = 10^6$ K at 1.05 $\mathrm{R_s}$. Then the electric potential V is given by Pannekoek-Rosseland and the altitude profiles of the moments depend on the VDFs of the particles (Pierrard and Lemaire 1996).

Figure 2.7 illustrates the temperature obtained with the radial distance with different VDFs. For all, the temperature increases, except for a single Maxwellian (blue) for which the temperature is constant. For Kappa VDFs (red: $\kappa = 3$, magenta: $\kappa = 6$, green: $\kappa = 10$), the temperature increases up to higher values for lower κ. For a sum of two Maxwellians (black), the temperatures increases up to T_1 (here chosen to be 10^7 K) with a slope that depends on the values of n_0, n_1, T_0, T_1 and V.

Note that the same argument $mv^2/2k_BT_0$ is used in the different VDFs leading to $T(r_0) > T_0$ for the Kappa VDFs and when a second Maxwellian with a higher temperature is added. This is due to the effect of the enhanced population of suprathermal particles for distributions having the same core population. For the Kappa VDF, $T(r_0) = \kappa T_0/(\kappa - 3/2) > T_0$ where T_0 is the temperature used in the core Maxwellian. A same Kappa distribution (using the expression of Eq 2.10) with different κ values will have the same core, but more suprathermal tails with lower

values of κ, associated to higher temperatures. This can lead to a misestimation of the temperature when the suprathermal tails are neglected by applying a Maxwellian distribution to fit the core instead of a Kappa distribution including the power law tails (Nicolaou and Livadiotis 2016).

The factor $\kappa - 3/2$ at the denominator shows clearly that the temperature can be calculated only if $\kappa > 3/2$. More generally, Kappa distributions need $\kappa > (l + 1)/2$ to ensure the convergence of the moments of order l, which means that we need $\kappa > 3/2$ to obtain a finite temperature and $\kappa > 2$ to estimate the heat flux of an anisotropic Kappa VDF (Pierrard and Lemaire 1998). A regularized Kappa distribution has been established with a Maxwellian-like cut-off of the power-law tails that ensures the convergence of the moments of any order and restrains the velocities to realistic values $v < c$, less than the speed of light in vacuum (Lazar et al. 2020b).

Figure 2.8 shows the temperature increase when assuming $T_0 = 6000\,\mathrm{K}$ at 1 $\mathrm{R_s}$ and other values of the parameters associated to solar photospheric conditions at this distance. The temperature increase is then very sharp (as observed in the corona) for any Kappa distribution. It reaches $T = 10^6\,\mathrm{K}$ even with high value of $\kappa = 10$, while the temperature remains constant when the distribution is Maxwellian. This mechanism of coronal heating only due to the presence of the suprathermal particles, without need of any wave-particle interactions, has been shown in Pierrard and Lamy (2003).

Moreover, because $q(r)$ depends not only on the temperature T but also on the mass m of the particles, the temperature increase will be different for each minor ion species, considering that the electric potential is determined mainly by the protons and electrons. The temperature is higher for heavy ions than for protons, and with a factor that depends on the mass on charge m/Z ratio of the ions (Pierrard and Lamy 2003). This is in good agreement with the observations of heavy ion temperatures that are much higher than the proton temperature in the solar wind (Pierrard et al. 2004). We illustrate here the temperature increase for the solar atmosphere, although the same effects can be obtained for any stellar or planetary atmosphere (Pierrard and Lemaire 1996).

Density

Figure 2.9 shows the density decrease associated to different VDFs, starting from $r_0 = 1.05\,\mathrm{R_s}$ with $n_0 = 10^{12}\,\mathrm{cm^{-3}}$ and $T_0 = 10^6\,\mathrm{K}$. The density of the Maxwellian (in blue) decreases faster than the Kappa VDFs for a same T_0. When the parameter κ is small, the density decreases slower (see the red line for $\kappa = 3$). For a sum of two Maxwellians (see black line), the decrease depends on n_1 (here chosen to be $3 \times 10^{10}\,\mathrm{cm^{-3}}$) and T_1 (here chosen to be 10^7 K) and is always slower than the core Maxwellian alone.

Because the VDFs are isotropic, the bulk velocity and the heat flux are equal to zero for all these distributions. But this is not anymore the case above the exobase where a flux starts to escape from the atmosphere.

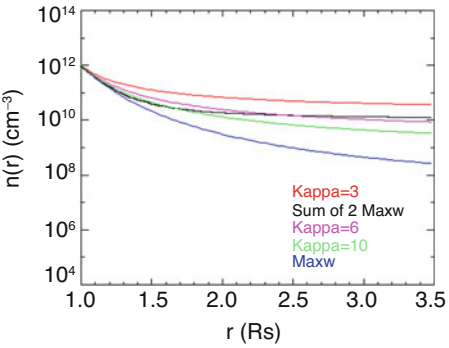

Fig. 2.9 Density decrease as a function of radial distance for different isotropic VDFs: Maxwellian (blue), sum of two Maxwellians (black), Kappa with $\kappa = 10$ (green), 6 (magenta) and 3 (red)

2.3.3 Anisotropic Distributions Above the Exobase

Observed VDFs in space plasmas are generally non-Maxwellian and have enhanced (suprathermal) high-energy tails (Maksimovic et al. 1997b). They are also often observed to be anisotropic. This is the case in the solar wind, even at distances as low as 0.3 AU: the protons have a VDF characterized by a tail or a beam in the direction parallel to the magnetic field (Pierrard and Voitenko 2013) and the electrons are characterized by a core, a halo and a field-aligned strahl population (Pierrard et al. 2001; Pierrard and Meyer-Vernet 2017). A single Maxwellian cannot fit such observations, while a Kappa distribution or a sum of two Maxwellians can better represent distributions with suprathermal tails (Lazar et al. 2017). As shown in Fig. 2.2, Kappa functions fit better the measured distributions than a sum of two Maxwellians, because the tails are observed to decrease as power laws. A sum of a core bi-Maxwellian + a bi-Kappa function (with 7 parameters n_c, $T_{c,\parallel}$, $T_{c,\perp}$, n_h, $T_{h,\parallel}$, $T_{h,\perp}$, κ_h) gives the best fits in the solar wind (Štverák et al. 2008) with a proportion of $n_1/n_0 \simeq 0.03$ in average and other interesting links between the parameters giving information on the mechanisms of formation of the tails (Pierrard et al. 2016, 2020). Drifting bi-Kappa distribution functions can also model features including field-aligned beams or drifting populations and the suprathermal populations.

In exospheric models (Fahr and Shizgal 1983), anisotropic distributions are logically obtained above the exobase, since the collisions can be neglected in this region and a flux of particles escapes from the atmosphere. The VDF becomes anisotropic because the particles with a high velocity escape from the atmosphere, leading to a non-zero flux. The most energetic particles escape and do not come back to the star or planet, so that the VDF is truncated, due to the empty part of particles with a high negative velocity (thus directed to the space body) (Pierrard 2012a). This form of VDF provides a simple explanation of the saturation or free streaming heat flux (Hollweg 1974). Such truncated VDFs are illustrated in Fig. 2.10 for a Maxwellian (in red) and a Kappa function with $\kappa = 3$ (in black).

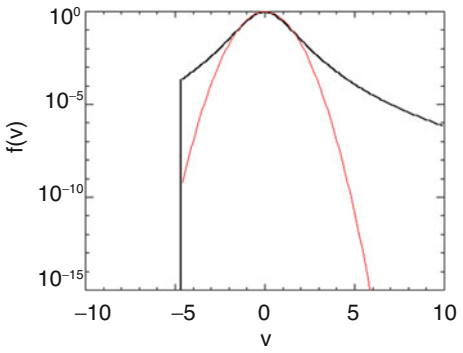

Fig. 2.10 Black: truncated Kappa distribution with $\kappa = 3$, red: truncated Maxwellian. Above the exobase, no electrons income from the interplanetary space with a velocity higher than the escape velocity in the direction of the star or planet. Here, v is the velocity normalized to the thermal speed $w = \sqrt{2k_BT/m}$

Solar Wind Acceleration

Exospheric models can be used to study the escape flux of planetary and stellar atmospheres, here for instance the solar wind. The particles with low energy are unable to escape in the interplanetary space when they are in an attractive potential, i.e., directed to the Sun. These ballistic particles come back to the Sun, so that the core of the particle VDF is symmetric. These particles do not contribute to any escape flux. The flux is only contributed by the particles with a velocity higher than the escape velocity v_l:

$$v_l = \sqrt{\frac{2GM}{r} - \frac{2Ze(V(r_0) - V(r))}{m}}, \tag{2.13}$$

with $G = 6.674 \times 10^{-11}$ m^3/(kg s^2) the universal gravity constant and $M = 1.99 \times 10^{30}$ kg, the mass of the Sun for the solar wind case (Pierrard 2009a for a review).

The flux F of Kappa VDFs is thus much higher than the flux of the Maxwellian with the same core, especially if the κ index is low, since the flux is contributed only by energetic particles. The density n, on the contrary, is not very different because it is mainly contributed by the low energy core particles. This causes a higher bulk velocity $u = F/n$ of solar wind particles when the electron VDF is a Kappa distribution (or any other distribution with an enhanced suprathermal tail) in comparison to a Maxwellian with the same core population (Pierrard and Lemaire 1996).

On Fig. 2.10, the normalized escape velocity for electrons is $v_l/w = \sqrt{mv_l^2/2k_BT} = 4.8$ at 3 Rs. The electrons with $v > v_l$ escape, thus they do not come back, and the VDF becomes anisotropic for high velocities since no particles coming from the interplanetary space are considered and we assume no collisions above the exobase. The electrons are always attracted to the Sun because the gravity and the electric force are directed to the space body. Protons and ions can be in a repulsive potential in case the electric force becomes larger than gravitational attraction above a certain radial distance r_{max} that depends on the mass and the electric charge of the ions (Pierrard and Lemaire 1996; Pierrard et al. 2004). The

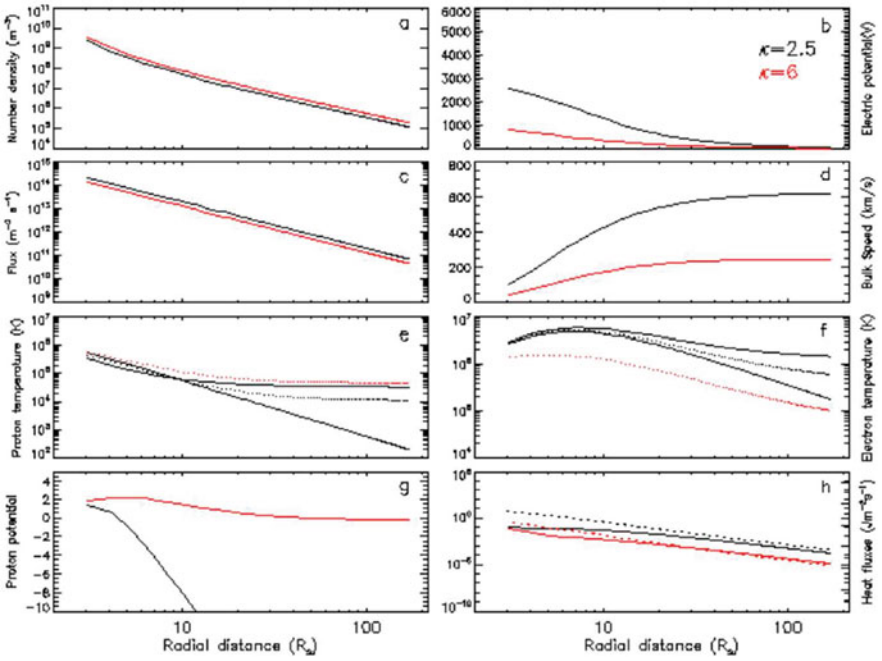

Fig. 2.11 Profiles of the moments for Kappa VDFs with $\kappa = 2.5$ in black and $\kappa = 6$ in red. Panel a. Density $n(r)$, b. Electric potential $V(r)$, c. Escape flux $F(r)$, d. Bulk speed $u(r)$, e. Proton temperature $T_p(r)$ (dotted: total, solid upper at high r: $T(r)$ parallel, lower solid at high r: $T(r)$ perpendicular), f. Electron temperature $T_e(r)$ (idem), g. Proton potential energy $\Phi_p(r)$, h. Heat flux $Q(r)$ (solid: protons, dotted: electrons). Obtained with the exospheric model from Pierrard and Pieters (2014)

electric potential $V(r)$ has to be calculated by imposing no net current, which can be non trivial in case of non monotonic potential (Lamy et al. 2003).

The Influence of Altitude

Figure 2.11 illustrates the profiles of the moments for two Kappa VDFs: low $\kappa = 2.5$ in black and higher $\kappa = 6$ in red in a purely exospheric model of the solar wind (Pierrard and Lemaire 1996; Pierrard and Pieters 2014). One can see that the flux $F(r)$ is higher for low kappa (panel c), the density $n(r)$ is on the contrary lower for low kappa (panel a), leading thus to higher bulk velocity $u(r) = F(r)/n(r)$ for low kappa (panel d).

An exobase at 3 Rs is used here. A lower exobase would even increase this bulk velocity (Lamy et al. 2003), even using the same temperature, which gives a natural explanation of high speed solar wind originating from the coronal holes where the density is lower than in the other regions of the corona.

The velocity increases with the radial distance and becomes supersonic for any value of κ, including for the particular case of $\kappa = \infty$ corresponding to the Maxwellian (Lemaire and Pierrard 2001). The relation between high bulk velocity

and low κ is indeed confirmed by observations (Maksimovic et al. 1997b). This acceleration is due to the high electric potential (panel b) associated to the high asymmetry of the distribution for high suprathermal tails (thus low κ).

The model gives a proton temperature (see panel e) perpendicular to the direction of the magnetic field higher than the parallel temperature at low distance, while it becomes the contrary at large distance. This is indeed observed, respectively in the solar corona from solar spectra, and in situ in the solar wind. For the electrons (panel f), the parallel temperature is larger than the perpendicular one, and the anisotropy increases with the radial distance. It becomes too large as compared to the observations at large distances (Berčič et al. 2019). This is probably related to the fact that exospheric models completely neglect any interactions between the different particles. The electron temperature has a maximum located in the low corona. The position of this maximum depends on the exobase and on the κ parameter, and is in good agreement with profiles deduced from solar eclipse observations (Pierrard and Pieters 2014).

Panel g shows that the kappa parameter has a high influence on the proton potential. Panel h illustrates the heat flux that is higher for low kappa (black), and slightly higher for electrons (dotted lines) than for protons (solid lines). Note that high electron heat flux and temperature anisotropies generate kinetic instabilities that limit the anisotropy of the distribution and are assumed to be responsible of the observed scattering of the strahl into the halo population with the radial distance (Verscharen et al. 2019; Sun et al. 2020).

Such exospheric models based on Kappa distributions can be used to make solar wind predictions using appropriate boundary conditions at low radial distances deduced from photospheric magnetograms (Pierrard and Pieters 2014; Moschou et al. 2017), and compare with solar wind observations more and more precise with recent years (see Rouillard et al. 2021 and references therein).

A sum of two Maxwellians with different temperatures also lead to such acceleration (Zouganelis et al. 2005), because it is physically due to the enhanced population of suprathermal particles. These effects associated to Kappa distributions are illustrated here for the solar case, but the same effects appear also for planetary atmospheres like those of the Earth and Mars (Pierrard 2003), of the giant planets and their moons (Pierrard 2009b; Tucker et al. 2016; Gamborino and Wurz 2018), the terrestrial polar wind (Barghouthi et al. 2001), the terrestrial plasmasphere along closed magnetic field lines (Pierrard and Lemaire 2001), auroral regions (Pierrard et al. 2007), or other stars (Scudder 1992b).

2.4 Conclusions

In this chapter, we summarize some of the most important characteristics of the observed VDFs in space plasmas, and the consequences of Kappa distributions for stellar and planetary atmospheres. At low altitude where there is no escape of particles (isotropic distributions), Kappa VDFs lead to an increase of the

temperature, without need of any other heating source (Pierrard 2012c). The simple presence of an enhanced population of suprathermal particles (even with a sum of two Maxwellians) can explain the heating of the solar corona. This effect can be generalized to all stars or planets, if an enhanced population of suprathermal particles (in comparison to a Maxwellian distribution with the same core) is present. Above the exobase (thus in the region where particles start to escape), the presence of suprathermal particles highly accelerates the wind. For the Sun's case, it explains the high bulk velocity observed in the fast solar wind escaping from the coronal holes, where the density temperature is lower than in other regions of the corona, but where the κ index is generally observed to be lower. These effects of Kappa distributions have revolutionized the physics of space plasmas by generalizing the particular Maxwellian case to more realistic distributions observed to have an enhanced suprathermal population decreasing as a power law of the velocity in ionized atmospheres.

Acknowledgments The authors acknowledge support from BIRA-IASB, STCE, UCLouvain, the Katholieke Universiteit Leuven and Ruhr-University Bochum. These results were obtained in the framework of the projects SCHL 201/35-1 (DFG-German Research Foundation) and G0A2316N (FWO-Vlaanderen). VP thanks the FED-tWIN project ENERGY.

References

B. Anderson, R. Skoug, J. Steinberg, D. McComas, J. Geophys. Res. Space Phys. **117**(A4), A04107 (2012). https://doi.org/10.1029/2011JA017269

M.R. Bakrania, I.J. Rae, A.P. Walsh, D. Verscharen, A.W. Smith, T. Bloch, C.E.J. Watt, A&A **639**, A46 (2020). https://doi.org/10.1051/0004-6361/202037840

I. Barghouthi, V. Pierrard, A.R. Barakat, J. Lemaire, Astrophys. Space Sci. **277**(3), 427 (2001). https://doi.org/10.1023/A:1012536114212

L. Berčič, M. Maksimović, S. Landi, L. Matteini, MNRAS **486**(3), 3404 (2019). https://doi.org/10.1093/mnras/stz1007

K. Chotoo, N.A. Schwadron, G.M. Mason, T.H. Zurbuchen, G. Gloeckler, A. Posner, L.A. Fisk, A.B. Galvin, D.C. Hamilton, M.R. Collier, J. Geophys. Res. Space Phys. **105**(A10), 23107 (2000). https://doi.org/10.1029/1998JA000015

S.P. Christon, D.J. Williams, D.G. Mitchell, L.A. Frank, C.Y. Huang, J. Geophys. Res. **94**(A10), 13409 (1989). https://doi.org/10.1029/JA094iA10p13409

M.R. Collier, D.C. Hamilton, G. Gloeckler, P. Bochsler, R.B. Sheldon, Geophys. Res. Lett. **23**(10), 1191 (1996). https://doi.org/10.1029/96GL00621

A.V. Eyelade, M. Stepanova, C.M. Espinoza, P.S. Moya, Astrophys. J. Suppl. Ser. **253** 34 (2021). https://doi.org/10.3847/1538-4365/abdec9

H.J. Fahr, B. Shizgal, Rev. Geophys. **21**(1), 75 (1983). https://doi.org/10.1029/RG021i001p00075

L.A. Fisk, G. Gloeckler, J. Geophys. Res. Space Phys. **119**(11), 8733 (2014). https://doi.org/10.1002/2014JA020426

D. Gamborino, P. Wurz, Planet. Space Sci. **159**, 97 (2018). https://doi.org/10.1016/j.pss.2018.04.021

C.M. Hammond, W.C. Feldman, D.J. McComas, J.L. Phillips, R.J. Forsyth, A&A **316**, 350 (1996)

J.V. Hollweg, J. Geophys. Res. **79**, 3845 (1974). https://doi.org/10.1029/JA079i025p03845

M.K. James, S.M. Imber, J.M. Raines, T.K. Yeoman, E.J. Bunce, J. Geophys. Res. Space Phys. **125**(6), e2019JA027352 (2020). https://doi.org/10.1029/2019JA027352

R.A. López, M. Lazar, S.M. Shaaban, S. Poedts, P.S. Moya, Astrophys. J. **900**(2), L25 (2020). https://doi.org/10.3847/2041-8213/abaf56
H. Lamy, V. Pierrard, M. Maksimovic, J. Lemaire, J. Geophys. Res. **108**, 1047 (2003). https://doi.org/10.1029/2002JA009487
M. Lazar, V. Pierrard, S. Poedts, R. Schlickeiser, in *Multi-Scale Dynamical Processes in Space and Astrophysical Plasmas*, ed. by M.P. Leubner, Z. Vörös (Springer Berlin Heidelberg, Berlin, Heidelberg, 2012a), pp. 97–107. https://doi.org/10.1007/978-3-642-30442-2_12
M. Lazar, R. Schlickeiser, S. Poedts, in *Exploring the Solar Wind*, ed. by M. Lazar (IntechOpen Publishing, Rijeka, 2012b), pp. 241–260. https://doi.org/10.5772/39281
M. Lazar, J. Pomoell, S. Poedts, C. Dumitrache, N.A. Popescu, Sol. Phys. **289**(11), 4239 (2014). https://doi.org/10.1007/s11207-014-0558-y
M. Lazar, S. Poedts, H. Fichtner, A&A **582**, A124 (2015). https://doi.org/10.1051/0004-6361/201526509
M. Lazar, H. Fichtner, P. Yoon, A&A **589**, A39 (2016). https://doi.org/10.1051/0004-6361/201527593
M. Lazar, V. Pierrard, S. Shaaban, H. Fichtner, S. Poedts, A&A **602**, A44 (2017). https://doi.org/10.1051/0004-6361/201630194
M. Lazar, K. Scherer, H. Fichtner, V. Pierrard, A&A **634**, A20 (2020a). https://doi.org/10.1051/0004-6361/201936861
M. Lazar, V. Pierrard, S. Poedts, H. Fichtner, A&A **642**, A130 (2020b). https://doi.org/10.1051/0004-6361/202038830
J. Lemaire, V. Pierrard, Astrophys. Space Sci. **277**, 169 (2001). https://doi.org/10.1023/A:1012218600882
M. Maksimovic, V. Pierrard, J. Lemaire, A&A **324**, 725 (1997a)
M. Maksimovic, V. Pierrard, P. Riley, Geophys. Res. Lett. **24**(9), 1151 (1997b). https://doi.org/10.1029/97GL00992
M. Maksimovic, I. Zouganelis, J.Y. Chaufray, K. Issautier, E.E. Scime, J.E. Littleton, E. Marsch, D.J. McComas, C. Salem, R.P. Lin, H. Elliott, J. Geophys. Res. **110**(A9), A09104 (2005). https://doi.org/10.1029/2005JA011119
M. Maksimovic, S.D. Bale, L. Berčič, J.W. Bonnell, A.W. Case, T.D.D. Wit, K. Goetz, J.S. Halekas, P.R. Harvey, K. Issautier, J.C. Kasper, K.E. Korreck, V.K. Jagarlamudi, N. Lahmiti, D.E. Larson, A. Lecacheux, R. Livi, R.J. MacDowall, D.M. Malaspina, M.M. Martinović, N. Meyer-Vernet, M. Moncuquet, M. Pulupa, C. Salem, M.L. Stevens, Š. Štverák, M. Velli, P.L. Whittlesey, Astrophys. J. Suppl. Ser. **246**(2), 62 (2020). https://doi.org/10.3847/1538-4365/ab61fc
N. Meyer-Vernet, in *Basics of the Solar Wind*. Cambridge Atmospheric and Space Science Series (Cambridge University Press, Cambridge, 2007). https://doi.org/10.1017/CBO9780511535765
S.P. Moschou, V. Pierrard, R. Keppens, J. Pomoell, Sol. Phys. **292**, 1 (2017). https://doi.org/10.1007/s11207-017-1164-6
G. Nicolaou, G. Livadiotis, Astrophys. Space Sci. **361**, 359 (2016). https://doi.org/10.1007/s10509-016-2949-z
G. Nicolaou, G. Livadiotis, R.T. Wicks, Entropy **22**(212), 1 (2020). https://doi.org/10.3390/e22020212
S. Olbert, in *Physics of the Magnetosphere*, vol. 10, ed. by R.D.L. Carovillano, J.F. McClay (1968), p. 641. https://doi.org/10.1007/978-94-010-3467-8_23
V. Pierrard, Planet. Space Sci. **51**, 319 (2003). https://doi.org/10.1016/S0032-0633(03)00014-X
V. Pierrard, *L'environnement spatial de la Terre* (Presses Universitaires de Louvain, Louvain-La-Neuve, 2009a)
V. Pierrard, Planet. Space Sci. **57**, 1260 (2009b). https://doi.org/10.1016/j.pss.2009.04.011
V. Pierrard, in *Exploring the Solar Wind*, ed. by M. Lazar (IntechOpen, Rijeka, 2012a), pp. 221–240. https://doi.org/10.5772/2079
V. Pierrard, ICNS Ann. Int. Astrophys. Conf. Proc. **1436**, 61 (2012b). https://doi.org/10.1063/1.4723591
V. Pierrard, Space Sci. Rev. **172**, 315 (2012c). https://doi.org/10.1007/s11214-011-9743-6

V. Pierrard, H. Lamy, Sol. Phys. **216**, 47 (2003). https://doi.org/10.1023/A:1026157306754
V. Pierrard, M. Lazar, Sol. Phys. **267**, 153 (2010). https://doi.org/10.1007/s11207-010-9640-2
V. Pierrard, J. Lemaire, J. Geophys. Res. **103**, 7923 (1996). https://doi.org/10.1029/95JA03802
V. Pierrard, J. Lemaire, J. Geophys. Res. **103**, 4117 (1998). https://doi.org/10.1029/97JA02665
V. Pierrard, J. Lemaire, J. Atmos. Sol. Terr. Phys. **633**, 1261 (2001). https://doi.org/10.1029/95JA03802
V. Pierrard, N. Meyer-Vernet, in *Kappa Distributions: Theory and Applications in Plasmas*, ed. by G. Livadiotis (Elsevier, Amsterdam, 2017), pp. 465–479. https://doi.org/10.5772/2079
V. Pierrard, M. Pieters, J. Geophys. Res. **119**, 9441 (2014). https://doi.org/10.1002/2014JA020678
V. Pierrard, Y. Voitenko, Solar Phys. **288**, 355 (2013). https://doi.org/10.1007/s11207-013-0294-8
V. Pierrard, M. Maksimovic, J. Lemaire, Astrophys. Space Sci. **277**, 195 (2001). https://doi.org/10.1023/A:1012218600882
V. Pierrard, H. Lamy, J. Lemaire, J. Geophys. Res. **109**, A02118 1 (2004). https://doi.org/10.1029/2003JA010069
V. Pierrard, G. Khazanov, J. Lemaire, J. Atmos. Sol. Terr. Phys. **69**(16), 2048 (2007). https://doi.org/10.1016/j.jastp.2007.08.005
V. Pierrard, M. Lazar, R. Schlickeiser, Sol. Phys. **269**, 421 (2011). https://doi.org/10.1007/s11207-010-9700-7
V. Pierrard, M. Lazar, S. Poedts, Š. Štverák, M. Maksimovic, P. Trávníček, Sol. Phys. **291**(7), 2165 (2016). https://doi.org/10.1007/s11207-016-0961-7
V. Pierrard, M. Lazar, S. Štverák, Sol. Phys. **295**, 151 (2020). https://doi.org/10.1007/s11207-020-01730-z
A. Rouillard, N. Viall, C. Vocks, Y. Wu, R. Pinto, M. Lavarra, L. Matteini, V. Pierrard, et al., *The Solar Wind* (AGU book, 2021). https://doi.org/10.1002/9781119815600.ch1
K. Scherer, H. Fichtner, M. Lazar, Europhys. Lett. **120**(5), 50002 (2017). https://doi.org/10.1209/0295-5075/120/50002
J.D. Scudder, Astrophys. J. **398**, 299 (1992a). https://doi.org/10.1086/171858
J.D. Scudder, Astrophys. J. **398**, 319 (1992b). https://doi.org/10.1086/171859
S.M. Shaaban, M. Lazar, S. Poedts, MNRAS **480**(1), 310 (2018). https://doi.org/10.1093/mnras/sty1567
B. Shizgal, Phys. Rev. E **97**(052144), 1 (2018). https://doi.org/10.1103/PhysRevE.97.052144
Š. Štverák, P. Trávníček, M. Maksimovic, E. Marsch, A.N. Fazakerley, E.E. Scime, J. Geophys. Res. **113**, A03103 (2008). https://doi.org/10.1029/2007JA012733
D. Summers, R.M. Thorne, Phys. Fluids B: Plasma Phys. **3**(8), 1835 (1991). https://doi.org/10.1063/1.859653
W.J. Sun, J.A. Slavin, R.M. Dewey, J.M. Raines, S.Y. Fu, Y. Wei, T. Karlsson, G.K. Poh, X. Jia, D.J. Gershman, Q.G. Zong, W.X. Wan, Q.Q. Shi, Z.Y. Pu, D. Zhao, Geophys. Res. Lett. **45**(16), 7933 (2018). https://doi.org/10.1029/2018GL079181
H. Sun, J. Zhao, W. Liu, H. Xie, D. Wu, Astrophys. J. **902**(1), 59 (2020). https://doi.org/10.3847/1538-4357/abb3ca
C. Tsallis, Phys. A **221**, 277 (1995). https://doi.org/10.1016/0378-4371(95)00236-Z
O.J. Tucker, W. Waalkes, V.M. Tenishev, R.E. Johnson, A. Bieler, M.R. Combi, A. Nagy, Icarus **272**, 290 (2016). https://doi.org/10.1016/j.icarus.2016.02.044
V.M. Vasyliunas, J. Geophys. Res. **73**(9), 2839 (1968). https://doi.org/10.1029/JA073i009p02839
D. Verscharen, B.D.G. Chandran, S.Y. Jeong, et al., Astrophys. J. **886**, L29 (2019). https://doi.org/10.3847/1538-4357/ab4c30
L.B. Wilson, L.J. Chen, S. Wang, S.J. Schwartz, D.L. Turner, M.L. Stevens, J.C. Kasper, A. Osmane, D. Caprioli, S.D. Bale, M.P. Pulupa, C.S. Salem, K.A. Goodrich, Astrophys. J. Suppl. Ser. **245**(2), 24 (2019). https://doi.org/10.3847/1538-4365/ab5445
L.B. Wilson III, M.L. Stevens, J.C. Kasper, K.G. Klein, B.A. Maruca, S.D. Bale, T.A. Bowen, M.P. Pulupa, C.S. Salem, Astrophys. J. Suppl. Ser. **236**(2), 41 (2018). https://doi.org/10.3847/1538-4365/aab71c

L.B. Wilson-III, L.J. Chen, S. Wang, S.J. Schwartz, D.L. Turner, M.L. Stevens, J.C. Kasper, A. Osmane, D. Caprioli, S.D. Bale, M.P. Pulupa, C.S. Salem, K.A. Goodrich, Astrophys. J. Suppl. Ser. **243**(1), 8 (2019). https://doi.org/10.3847/1538-4365/ab22bd

P.H. Yoon, Eur. Phys. J. Spec. Topics **229**, 819 (2020). https://doi.org/10.1140/epjst/e2020-900215-4

I. Zouganelis, N. Meyer-Vernet, S. Landi, M. Maksimovic, F. Pantellini, Astrophys. J. Lett. **626**(L117), 1151 (2005) https://doi.org/10.1086/431904